Proceedings of the Combustion Institute 41 (2025) 105917

Contents lists available at ScienceDirect

Proceedings of the Combustion Institute

journal homepage: www.elsevier.com/locate/proci

An analysis of the ignition of hydrogen/n-dodecane dual-fuel mixing layers at engine-relevant conditions

Shibo Gu [a,b,*], Armin Wehrfritz [c], Evatt R. Hawkes [a], Yunchao Wu [d], Tianfeng Lu [d], Haiou Wang [e,**]

[a] School of Mechanical and Manufacturing Engineering, University of New South Wales, Sydney, NSW 2052, Australia
[b] Taihang Laboratory, Chengdu 610299, PR China
[c] Department of Mechanical and Materials Engineering, University of Turku, Turku 20014, Finland
[d] Department of Mechanical Engineering, University of Connecticut, Storrs, CT 06269-3139, USA
[e] State Key Laboratory of Clean Energy Utilization, Zhejiang University, Hangzhou 310027, PR China

ARTICLE INFO

Keywords:
Dual fuel
Hydrogen
Two-stage ignition
Preferential diffusion

ABSTRACT

Hydrogen is attracting increasing attention as a clean-burning, carbon-neutral fuel in heavy-duty engine applications, which usually often operate by compression ignition. However, hydrogen cannot ignite on its own under typical conditions in these engines. To address this, the concept of hydrogen-diesel dual direct injection (H_2DDI) has been recently proposed in which hydrogen and diesel are introduced separately into the combustion chamber, with diesel providing the ignition source, leading to ignition occurring in stratified mixtures. This study employs numerical simulations to investigate the ignition of stratified mixtures in one-dimensional laminar mixing-layer configurations under engine-relevant conditions, where a *n*-dodecane fuel-rich stream is surrounded by an oxidiser stream with (dual-fuel/DF cases) and without (single fuel/SF cases) hydrogen. It is shown that the ignition of the DF cases is delayed compared to the SF cases because hydrogen consumes OH species during the low-temperature oxidation of *n*-dodecane. Unlike the SF cases, the DF cases exhibit a postponed initiation of the first-stage ignition relative to the most reactive ignition delay time observed in homogeneous reactor simulations. In both the SF and DF cases, diffusion-supported cool flames promote radical accumulation, accelerating the transition to the second-stage ignition. Furthermore, the study reveals that preferential diffusion effects in both the SF and DF cases, influenced by mixing conditions, significantly impact the ignition process, with the diffusion behaviours of different species playing distinct roles in the ignition of both stages. In particular, the preferential diffusion of *n*-dodecane is the dominant factor of overall preferential diffusion effects, delaying both the first and second-stage ignition, whereas the preferential diffusion of hydrogen only increases the maximum flame temperature.

1. Introduction

In response to stringent emission standards, hydrogen (H_2) has emerged as a promising alternative fuel for compression ignition (CI) engines. A practical approach is dual-fuel (DF) operation, wherein a hydrogen/air mixture is ignited through the autoignition of a pilot diesel injection. Direct Injection (DI), preferred over Port Fuel Injection (PFI) [1], mitigates the risks of knocking and pre-ignition by enabling precise control over fuel delivery. In recent experiments and simulations [2,3], it was demonstrated that the injection timing of hydrogen and hydrogen energy fractions affect engine efficiency, combustion phasing, NO_x emissions and wall heat loss. A notable example is a mid-load dual-fuel hydrogen-diesel direct injection (H_2DDI) engine with a 50% hydrogen energy share, achieving an indicated efficiency of 47% while managing a 40% increase in NO_x emissions compared to the diesel baseline [2]. In H_2DDI engines, DF combustion exhibits a complex interaction between chemical processes and transport phenomena, which is not yet fully understood. Hence, a comprehensive understanding of the DF ignition mechanism in thermally and compositionally stratified mixtures is crucial for optimising engine performance parameters.

Diesel surrogate ignition involves distinct low-temperature chemistry (LTC) and high-temperature chemistry (HTC) pathways, which are expected to be influenced by hydrogen addition. Several studies [4,5] of H_2/*n*-C_7H_{16} mixtures have been carried out in low-pressure ($\leq$ 10 bar)

* Corresponding author at: School of Mechanical and Manufacturing Engineering, University of New South Wales, Sydney, NSW 2052, Australia.
** Corresponding author.
E-mail addresses: shibo_gu@163.com (S. Gu), wanghaiou@zju.edu.cn (H. Wang).

https://doi.org/10.1016/j.proci.2025.105917
Received 20 June 2025; Accepted 1 October 2025
Available online 15 October 2025

conditions to understand the effects of H_2 addition on the ignition of n-C_7H_{16}. It was shown that adding hydrogen retards the first-stage ignition because OH, which plays a key part in the H abstraction of the LTC pathway, is consumed by H_2 via reactions $H_2 + OH \rightleftharpoons H + H_2O$ and $H + O_2 \rightleftharpoons HO_2$. However, the chemical interaction between diesel surrogates and hydrogen might differ at different ambient and mixture conditions, especially at high-temperature and high-pressure engine conditions. Furthermore, these interactions are likely affected by stratification, discussed next.

The ambient thermal and compositional conditions in a practical CI engine are highly stratified, suggesting that transport effects likely influence the ignition mechanism. Several studies focused on high-temperature, single-stage ignition [6,7]. Autoignition was observed as a "spotty" event in space and time partly due to the fluctuations of the scalar dissipation rate. Ignition kernels usually occur at a low scalar dissipation rate and composition that is close to the most reactive mixture fraction calculated from homogeneous reactors, i.e. the mixture having the shortest ignition delay. The competition between the dominant chemistry responsible for the growth of radical pools and the dissipation of heat and species determines the subsequent evolution of these kernels. With the recent development of employing low-temperature combustion techniques to optimise conventional diesel engines, the role of low-temperature combustion and two-stage ignition has been identified. It has been shown in direct numerical simulations of dimethyl ether (DME)/air mixing layers that diffusion causes acceleration of the cool flame relative to first stage ignition timings expected from homogeneous reactors, which then results in accelerated high temperature ignition [8], a phenomenon that has been referred to as a "cool flame wave" in analysis of results from a flamelet model [9]. However, it is unclear how any of these mechanisms associated with stratification are affected by the presence of hydrogen.

Preferential diffusion, arising from the high diffusivity of hydrogen relative to large hydrocarbons, is a critical factor in hydrogen–diesel dual-fuel combustion. Several studies focused on the non-premixed combustion of hydrogen-enriched fuels. For instance, the ignition of H_2/CH_4 binary fuel blends was examined in a non-premixed counterflow configuration [10]. The ignition of CH_4/air is accelerated with H_2 addition. Preferential diffusion of H_2 induces more reactive H_2 within the ignition kernel, thereby amplifying this ignition enhancement. Similarly, the ignition process of H_2 and iso-octane blends was investigated in a one-dimensional (1D) mixing-layer configuration [11] . The ignition delay time of the system is reduced because the preferential diffusion of H_2 increases the local concentration of H_2 in the ignition kernel. Nevertheless, no attempt has been made on the preferential diffusion effects on the two-stage ignition of hydrogen/n-dodecane (n-$C_{12}H_{26}$) in dual-fuel combustion.

In conclusion, previous studies on H_2 have primarily examined its role as an additive in fuel blends and at atmospheric or relatively low pressures, differing significantly from H_2-based DF engines where the charge is stratified under engine-relevant conditions. These limitations largely stem from the lack of validated DF mechanisms capable of capturing LTC–HTC coupling at high pressure and the fact that systematic attention to LTC and cool flames in stratified mixtures has only recently emerged. To address this gap, this work investigates H_2/n-$C_{12}H_{26}$ ignition under DF engine conditions using a newly developed and validated DF mechanism in 1D laminar mixing-layer simulations, a simplified framework that omits engine-specific complexities yet enables clear analysis of fundamental ignition processes. The objectives are threefold: (i) to elucidate the mechanisms of H_2/n-$C_{12}H_{26}$ interaction during ignition of stratified mixtures at engine conditions; (ii) to identify the role of diffusion in the ignition process; and (iii) to examine the effects of preferential diffusion on ignition.

2. Numerical methods and configurations

A spatially evolving 1D mixing layer configuration is depicted in Fig. 1. The domain length is 2 mm, discretised with a uniform grid size of 1 μm, as verified in the Supplementary Material. The thickness of the mixing layer, δ, in the baseline case is set to 50 μm. The boundary conditions are non-reflecting outflow in the y-direction. To determine the composition across the mixing layer, we consider adiabatic mixing between two reference streams that are set to mimic ECN Spray A conditions [12] . The oxidiser stream, having mixture fraction $\xi = \xi_{ox} = 0$, has a temperature of 900 K, and is either the ECN standard oxidiser mixture of 15% O_2 and 85% N_2 by volume in single-fuel (SF) cases, or a hydrogen-enriched mixture of this oxidiser and some hydrogen in dual-fuel cases (details later). The fuel stream, having mixture fraction $\xi = 1$, is composed of liquid n-dodecane at 363 K. Our simulations consider a mixing layer between ξ_{ox}, i.e. pure oxidiser, and a partially mixed fuel-air stream at $\xi = \xi_f = 0.3$, i.e. the simulations consider a peak mixture-fraction condition representative of a local in a jet downstream of the liquid injection, breakup, evaporation, and mixing with the oxidiser stream, similar to other previous studies that did not consider hydrogen enrichment [13]. Our simulations prescribe a hyperbolic tangent profile of mixture fraction (Fig. 1), and local states including temperature are determined by adiabatic mixing between the reference streams according to the local mixture fraction. This results in a peak temperature of 575 K at ξ_f. For the DF cases, the hydrogen equivalence ratio in oxidiser stream is set to have $\phi = 0.3$, representing ultra-lean H_2 operation of hydrogen internal combustion engines proposed to reduce NO_x emissions [14], and chosen here as a representative condition that highlights preferential diffusion effects (analysed in Section 3.3) while remaining computationally feasible for 1D simulations. This results in n-dodecane, O_2, N_2 and H_2 with a temperature T_f =587 K at ξ_f. The pressure, P, in all cases was set to 60 atm, corresponding to ECN Spray A conditions. The temperatures and compositions at ξ_{ox} and ξ_f are given in Table 1.

The simulations are carried out with S3D [15], using high-order, non-dissipative numerical methods on a uniform Cartesian grid. The time integration is performed through a six-stage fourth-order explicit Runge–Kutta method. The spatial discretisation uses an eighth-order central differencing scheme, and spurious high-frequency fluctuations in the solution are removed by a tenth-order filter. The Navier–Stokes characteristic boundary conditions (NSCBC) are used at the outflow boundaries. The chemical mechanism employed in this study is tailored to capture the combustion characteristics of hydrogen and n-dodecane. It originates from a 54-species and 269-reaction skeletal mechanism [16]. To enhance its applicability to hydrogen combustion, the hydrogen oxidation pathways were replaced with reactions from the AramcoMech 3.0 mechanism [17], achieving improved agreement with experimental measurements of laminar flame speeds and ignition delay times. The final 35-species and 268-reaction reduced mechanism, derived through quasi-steady-state approximations, maintains high accuracy in predicting ignition delay, flame speed, and key species profiles under dual-fuel combustion conditions. A detailed validation is provided in the Supplementary Material.

3. Results and discussion

3.1. Ignition process in homogeneous reactors

The configuration of constant pressure homogeneous reactors is used for studying hydrogen addition effects on n-dodecane ignition using Cantera [18]. The first-stage, second-stage ignition delay time (τ_1^{0D}, τ^{0D}) and adiabatic temperature (T_{ad}) as a function of mixture fraction (ξ) in the SF and DF cases are shown in Fig. 2. The values of τ_1^{0D} and τ^{0D} are defined as the corresponding timing of the maximum consumption rate of RO_2 and H_2O_2, respectively. This definition is in good agreement with the widely used definition based on maximum

Table 1
The temperatures and compositions at $\xi = \xi_{ox} = 0$ and $\xi = \xi_f = 0.3$.

	$\xi = \xi_f = 0.3$ (*n*-dodecane/oxidiser premixture)						$\xi = \xi_{ox} = 0$ (oxidiser)				
	T_f (K)	P (atm)	$X_{n-C_{12}H_{26},f}$	$X_{H_2,f}$	$X_{O_2,f}$	$X_{N_2,f}$	T_{ox} (K)	P (atm)	$X_{H_2,ox}$	$X_{O_2,ox}$	$X_{N_2,ox}$
SF	575	60	7%	0	14%	79%	900	60	0	15%	85%
DF	587	60	6%	8%	13%	73%	900	60	8%	14%	78%

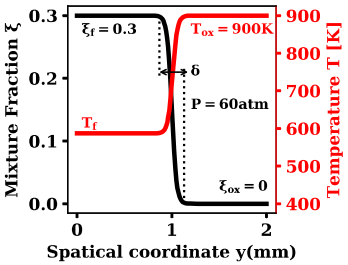

Fig. 1. Schematic of the 1D mixing layer configuration.

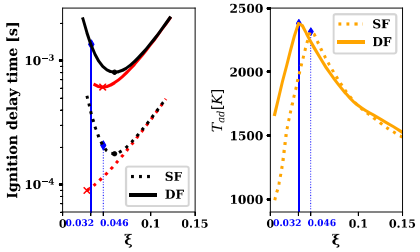

Fig. 2. The first-stage (red lines), second-stage (black lines) ignition delay time (left) and adiabatic temperature (right) over mixture fraction space in the context of homogeneous reactors; cross markers denote the most reactive first-stage ignition delay time ($\tau^{0D}_{1,mr}$) and mixture fraction ($\xi^{0D}_{1,mr}$); circle markers denote the most reactive second-stage ignition delay time (τ^{0D}_{mr}) and mixture fraction (ξ^{0D}_{mr}); diamond markers denote the stoichiometric mixture fraction and ignition time (ξ_{st}, τ^{0D}_{st}).

heat release rate (HRR) peak or maximum temperature rise rate, as the maximum consumption rates of RO_2 and H_2O_2 are related to major exothermic reactions [19], which contribute significantly to the HRR and temperature rise. It is shown that compared to the SF case, hydrogen addition significantly delays the first-stage ignition and shifts the most reactive first-stage ignition delay time ($\tau^{0D}_{1,mr}$) to a richer mixture, which leads to the increase in the second-stage ignition delay time. Also, the value of stoichiometric mixture fraction (ξ_{st}) is lower in the DF case, but the most reactive second-stage ignition occurs in the same mixture fraction (ξ^{0D}_{mr}), which is considered a coincidence resulting from local mixture composition and temperature. In both cases, T_{ad} first increases and then decreases with increasing mixture fraction, and the maximum value occurs at stoichiometry. The value of T_{ad} is higher at stoichiometry in the DF case than in the SF case.

For further investigation of the prolonged first-stage ignition in the DF case, a sensitivity analysis of τ^{0D}_1 is performed and presented in Fig. 3 to identify the controlling reactions, where the positive and negative coefficients denote inhibiting and promoting effects, respectively. It is seen that adding H_2 into the *n*-dodecane/air mixture mainly promotes the reactions $H_2 + OH \rightleftharpoons H + H_2O$, $H + O_2 + (M) \rightleftharpoons HO_2 + (M)$, and $2\,HO_2 \rightleftharpoons H_2O_2 + O_2$, which therefore decelerates the H-abstraction reactions of *n*-dodecane by consuming OH radicals (such as $n-C_{12}H_{26} + OH \rightleftharpoons H_2O + SXC_{12}H_{25}$, $n-C_{12}H_{26} + OH \rightleftharpoons H_2O + S_3XC_{12}H_{25}$) and hence suppresses LTC.

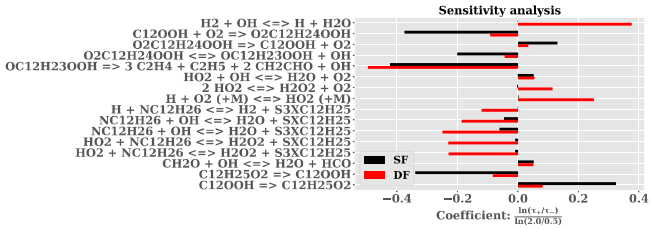

Fig. 3. The sensitivity analysis at the same mixture fraction ($\xi = 0.05$) in SF and DF baseline cases; the sensitivity coefficient is defined as $S = \frac{ln(\tau_{1+}/\tau_{1-})}{ln(k_+/k_-)} = \frac{ln(\tau_{1+}/\tau_{1-})}{ln(2.0/0.5)}$, where τ_{1+} and τ_{1-} represent first-stage ignition delay time with the reaction rate coefficient k_+ and k_- being artificially modified to 2.0 and 0.5 times of its original value.

3.2. Diffusion effects in 1D mixing layers

The degree of species diffusivity in a mixture is characterised by the Lewis number (Le), which is defined as the ratio of thermal diffusivity to species diffusivity. Deviations from the unity of the Lewis number result in preferential diffusion. To better understand the ignition process of SF and DF systems and the role of H_2 with the influence of mixing, a revised Lewis number approach is employed, in which species diffusion coefficients are adjusted. Six numerical simulation scenarios are designed, including a $Le \neq 1$ scenario where all species diffusion coefficients are calculated using a mixture-averaged approach [20], and a $Le = 1$ scenario where all species diffusion coefficients are equal to the thermal diffusion coefficient. To investigate the impact of diffusion, the $Le \neq 1$ scenario is compared to the zero-dimensional (0D) case in constant-pressure homogeneous reactors in this section. The preferential diffusion effect is examined by comparing the $Le \neq 1$ scenario with the $Le = 1$ scenario. Furthermore, to evaluate the preferential diffusion effects of key species, four additional scenarios are considered in which one of four species (i.e. *n*-$C_{12}H_{26}$, H_2, RO_2 and OH) retains its original species diffusion coefficient while the mass diffusion coefficients of all other species are set to the thermal diffusion coefficient (RO_2 and OH are selected as important intermediates in low and high-temperature chemistry, respectively). These cases, labelled as $Le_{NC_{12}H_{26}}$, Le_{H_2}, Le_{RO_2} and Le_{OH}, with the subscripts corresponding to the species for which non-unity Lewis number is retained, are compared with the $Le = 1$ scenario. A summary of all 1D simulation cases, including the variations in Lewis number models and mixing layer thicknesses, is provided in Table 2. The next section will discuss the preferential diffusion effects in more detail.

The distributions of HRR in the 0D and $Le \neq 1$ cases are illustrated in Fig. 4, highlighting the evolution of HRR over the mixture fraction ξ, along with markers indicating the most reactive locations and times for the first ($\xi^{0D}_{1,mr}$, $\tau^{0D}_{1,mr}$) and second (ξ^{0D}_{mr}, τ^{0D}_{mr}) stage as well as the stoichiometric mixture fraction and ignition time (ξ_{st}, τ^{0D}_{st}). The time t^* is normalised by the corresponding τ^{0D}_{mr}. In both the SF and DF cases, it is observed that heat release advances faster and further into rich mixtures in the 1D cases when compared to the corresponding 0D cases. This behaviour is consistent with earlier studies [21] on the ignition process of DME showing that the differences between 0D and two-dimensional simulations are due to the fact that LTC reaction

Table 2
Summary of 1D simulation cases.

	$D_{n\text{-}C_{12}H_{26}}$	D_{H_2}	D_{RO_2}	D_{OH}	D_k	δ (μm)
$Le \neq 1$	$D^{mix}_{n\text{-}C_{12}H_{26}}$	$D^{mix}_{H_2}$	$D^{mix}_{RO_2}$	D^{mix}_{OH}	D^{mix}_k	5, 10, 20, 30, 50, 70, 90, 100, 110, 130, 150
$Le = 1$	α	α	α	α	α	20, 50, 100
$Le_{n\text{-}C_{12}H_{26}}$	$D^{mix}_{n\text{-}C_{12}H_{26}}$	α	α	α	α	20, 50, 100
Le_{H_2}	α	$D^{mix}_{H_2}$	α	α	α	20, 50, 100
Le_{RO_2}	α	α	$D^{mix}_{RO_2}$	α	α	20, 50, 100
Le_{OH}	α	α	α	D^{mix}_{OH}	α	20, 50, 100

Note: k denotes all species other than n-$C_{12}H_{26}$, H_2, RO_2, and OH. The mixture-averaged diffusion coefficient for species i is defined as $D_i^{mix} = \frac{1-Y_i}{\sum_{j\neq i} X_j/D_{ij}}$ [20], where D_{ij} is the binary diffusion coefficient between species i and j, Y_i is the mass fraction of species i, and X_j is the mole fraction of species j. The thermal diffusivity is given by $\alpha = \lambda/(\rho C_p)$, where λ is the thermal conductivity, ρ is the density, and C_p is the specific heat capacity at constant pressure.

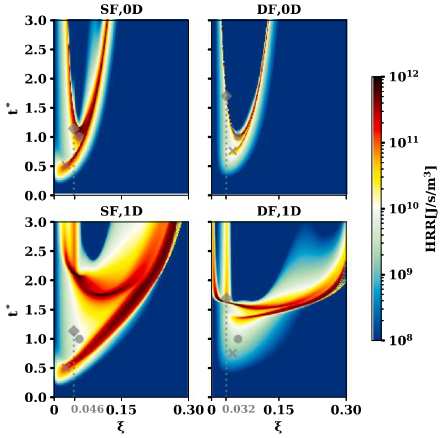

Fig. 4. HRR contour over mixture fraction ξ in 0D (top) and 1D $Le \neq 1$ (bottom) simulations; cross and circle markers denote the first- ($\xi^{0D}_{1,mr}$, $\tau^{0D}_{1,mr}$) and second-stage (ξ^{0D}_{mr}, τ^{0D}_{mr}) most reactive location and time, respectively; diamond markers denote the stoichiometric mixture fraction and ignition time (ξ_{st}, τ^{0D}_{st}).

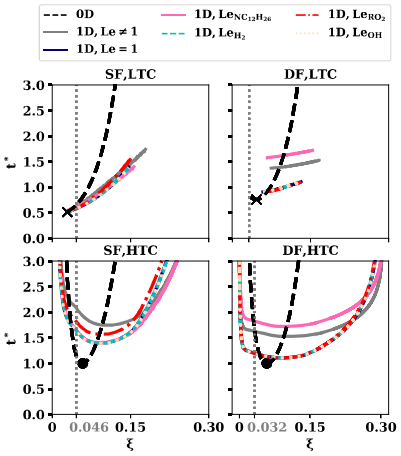

Fig. 5. Temporal evolution of LTC (upper row) and HTC (lower row) reaction fronts in SF (left) and DF (right) cases; dashed lines are the evolution of ignition delay times in 0D simulations; cross and circles denote ($\xi^{0D}_{1,mr}$, $\tau^{0D}_{1,mr}$) and (ξ^{0D}_{mr}, τ^{0D}_{mr}) locations, respectively; dotted vertical lines denote the stoichiometry.

fronts act as a diffusively supported flame structure, i.e. a cool flame. Furthermore, compared to the 1D SF case, the HRR contour is shown to extend to a much leaner mixture in the 1D DF case. While a two-stage ignition process is observed in both the SF and DF cases, there is a different response to molecular transport. The initiation of the first-stage ignition is close to $\tau^{0D}_{1,mr}$ in the 1D SF case, but is delayed in the 1D DF case. The second-stage ignition is initiated at a later time compared to τ^{0D}_{mr} in both the 1D SF and 1D DF cases. Also, the ignition at stoichiometry is delayed in the 1D SF case and is slightly accelerated in the 1D DF case compared to τ^{0D}_{st}. The discrepancies in ignition delay times between 0D and 1D simulations described above are caused by distinct control mechanisms. In 0D simulations, ignition delay times are exclusively controlled by chemical reactions. In 1D simulations, the introduction of spatial gradients in mixture fraction and temperature enables diffusion to influence the ignition process. Autoignition occurs at specific locations where favourable conditions emerge due to the interplay between species and heat transport, modifying the temporal and spatial characteristics of ignition compared to the kinetically controlled 0D cases.

LTC and HTC reaction fronts, which can be represented by the maximum consumption rates of RO_2 and H_2O_2 (as same as the ignition definition in 0D), are tracked over time in the six scenarios mentioned above, shown in Fig. 5. The first- and second-stage ignition delay times (τ_1^{1D} and τ^{1D}) in 1D simulations are defined as the occurrence timing of the first LTC and HTC reaction fronts. These timings coincide with the first and second occurrences of the maximum gradient of the maximum temperature. By comparing the $Le \neq 1$ scenario with the 0D scenario, it is seen that the trajectory of LTC reaction fronts in the SF cases is initially near the first-stage ignition curves of 0D simulations and gradually deviates. Particularly, LTC is accelerated compared to 0D simulations, and this acceleration becomes more pronounced in richer mixtures, consistent with earlier remarks regarding the cool flame. In the DF case, the occurrence timing of LTC reaction fronts at the same mixture fraction is prolonged at first and then shortened compared to first-stage ignition delay times in 0D simulations. Regarding HTC reaction fronts, their trajectories are shown in Fig. 5, which are highly influenced by the LTC, and also deviate from the curve of 0D second-stage ignition delay times. The behaviours of other scenarios will be discussed in the next section.

Identifying different ignition modes of reaction fronts can elaborate the transport effects from a different angle and provide theoretical support for determining simulation models. Heat and mass diffusion effects can be divided into (1) passive scalar dissipation, where the initial inhomogeneity introduced by stratification and turbulence prior to ignition; (2) the molecular diffusion taking effects within the ignition fronts and controls the different regimes [22]. The regimes of a reaction front propagating through a stratified mixture contain four ignition modes, of which volumetric autoignition (spontaneous ignition mode) and flame propagation mode (deflagration mode) are of primary interest in the current case. Volumetric autoignition mode describes sequential propagation in consecutive mixtures due to the differences in ignition delay times determined by chemistry only. The flame propagation mode denotes a premixed flame propagating under the influence of molecular diffusion. Several studies were performed to identify these two ignition modes by examining the Damköhler number [13,23]. Here,

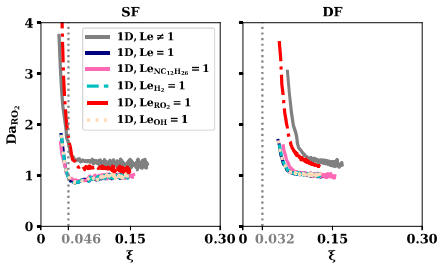

Fig. 6. Evolution of Da_{RO_2} along ξ for LTC reaction fronts; dashed vertical lines denote the stoichiometry.

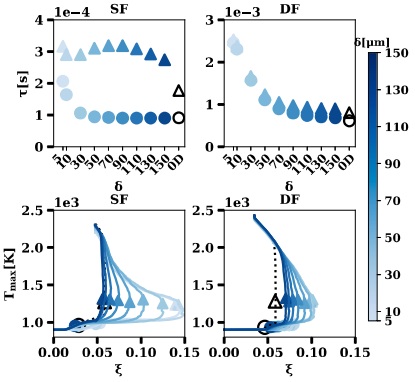

Fig. 7. Ignition delay times with varied δ (upper row); maximum temperature evolution alongside mixture fraction space (lower row); filled circles and triangles represent τ_1^{1D} and τ^{1D} in the upper row, and ξ_1^{1D} and ξ^{1D} in the lower row; unfilled circles and triangles denote $\tau_{1,mr}^{0D}$ and τ_{mr}^{0D} in the upper row, and $\xi_{1,mr}^{0D}$ and ξ_{mr}^{0D} in the lower row.

the Damköhler number of RO_2 (Da_{RO_2}) is selected, which is defined as $Da_{\mathrm{RO}_2} = \frac{\max|\omega_{\mathrm{RO}_2}|}{\max|-\nabla\cdot(\rho Y_{\mathrm{RO}_2}\mathbf{V}_{\mathrm{RO}_2})|}$, where ω_{RO_2} is the RO_2 reaction rate and $\mathbf{V}_{\mathrm{RO}_2}$ is the diffusion velocity. The reaction front with Da_{RO_2} greater than unity is regarded as spontaneous ignition controlled by chemistry, and the reaction front with Da_{RO_2} approximately equal to unity propagates as a deflagration flame (i.e. cool flame) strongly affected by molecular diffusion. The trajectories of Da_{RO_2} for the SF and DF cases are illustrated in Fig. 6. At the $Le \neq 1$ scenario, the value of Da_{RO_2} is larger than 1 firstly and then fluctuates around 1, indicating reaction fronts transit from autoignition to cool flame.

Diffusion effects on the ignition process are further analysed in Fig. 7, which illustrates ignition delay times for varying mixing layer thicknesses δ (upper row) and the evolution of maximum temperature along the mixture fraction space (lower row), with markers indicating the corresponding ignition times and locations for both 0D and 1D simulations. Three points can be made from the figure. Firstly, the first-stage ignition delay time displays different responses to varying diffusive intensity in the SF and DF cases. In the SF case, τ_1^{1D} and ξ_1^{1D} are the highest at small δ and level off with increasing values of δ. In the DF case, τ_1^{1D} and ξ_1^{0D} decrease monotonically with increasing δ, suggesting a more significant strengthening of inhibition effects due to enhanced diffusion. This phenomenon may arise from the increased diffusion leading to higher losses of heat and radicals produced during the ignition process. Although the same series of δ are selected in the SF and DF case, the different sensitivity of τ_1^{1D} to the variation of δ is due to different levels of scalar dissipation rate. For instance, with $\delta = 5\,\mu\mathrm{m}$, the scalar dissipation rate at the stoichiometry is $847\,\mathrm{s}^{-1}$ at $t^* = 0$ in the SF case, and $641\,\mathrm{s}^{-1}$ in the DF case. Secondly, the path of maximum temperature below the turning point in the richest mixture fraction, which is governed by LTC, extends to a much richer mixture compared with 0D simulations. The phenomenon has been elaborated as the propagation of cool flame in the above ignition mode analysis. In the SF and DF cases, increasing diffusion (decreasing δ) promotes the movement of the LTC region (cool flame) to the richer mixture (except for $\delta = 5\,\mu\mathrm{m}$). Finally, τ^{1D} has different trends in SF and DF cases. For the SF case, the trend of τ^{1D} with increasing δ is non-monotonic, exhibiting varied responses to different levels of diffusion. In the DF case, τ^{1D} decreases with increasing δ even with the assisted promoting effect of cool flame, owing to the strong influence by the escalating trend of τ_1^{1D}.

3.3. Preferential diffusion effects in 1D mixing layers

In the 1D cases, the Lewis numbers of n-$C_{12}H_{26}$, H_2, RO_2 and OH vary throughout the flame with ranges of 2.81–4.33, 0.19–0.33, 2.93–4.43, and 0.49–0.82, respectively. As shown in Fig. 5, differences between the $Le \neq 1$ and $Le = 1$ scenarios are observed for LTC and HTC reaction fronts in both the SF and DF cases, indicating that preferential diffusion occurs at the current mixing conditions. It is noted that the preferential diffusion of individual species shows different behaviours in the SF and DF cases. Particularly, in the SF case, the preferential diffusion of n-$C_{12}H_{26}$ is negligible for LTC and HTC reaction fronts except at richer mixtures. The preferential diffusion of RO_2 is negligible for LTC reaction front and decelerates the initiation of HTC reaction front. In the DF case, the preferential diffusion of n-$C_{12}H_{26}$ slows down the initiation of LTC and HTC reaction fronts due to its low diffusivity. The preferential diffusion of RO_2 is insignificant for LTC and HTC reaction fronts. Also, the preferential diffusion of H_2 and OH shows no influence on the evolution of these reaction fronts in both the SF and DF cases. Additionally, the transition from autoignition to cool flame structures is also observed for various cases in Fig. 6.

The preferential diffusion effects show the different behaviours at different mixing conditions. The maximum temperature T_{max} is tracked for different cases with varying mixing layer thickness δ as shown in Fig. 8. In the SF case, the preferential diffusion effects gradually disappear at the first-stage ignition but remain significant at the second-stage ignition with increasing δ. It is observed that the first- and second-stage ignition are delayed in the $Le_{\mathrm{NC_{12}H_{26}}}$ scenario compared to the $Le = 1$ scenario when $\delta = 20\,\mu\mathrm{m}$, but this behaviour gradually disappears with increasing δ. The preferential diffusion of RO_2 does not impact the first-stage ignition but delays the second-stage ignition. The preferential diffusion of H_2 and OH has no impact on the first-stage and second-stage ignition. In the DF case, the preferential diffusion effects are more pronounced with decreasing δ for the two-stage ignition, where the preferential diffusion of n-$C_{12}H_{26}$ plays a dominant role, and the preferential diffusion of RO_2, H_2 and OH plays an insignificant role. It is also noticed that preferential diffusion of H_2 leads to a higher maximum flame temperature in both cases. The same conclusions are drawn when the hydrogen equivalence ratio in the oxidiser stream varies from 0.1 to 0.5, as shown in the Supplementary Material.

4. Conclusions

The ignition characteristics of DF mixtures were investigated using 0D homogeneous reactors and 1D laminar mixing layers, with n-dodecane as the fuel and a hydrogen-enriched oxidiser. Comparisons with SF combustion, where hydrogen was absent in the oxidiser, elucidated the effects of hydrogen addition. The 0D results indicate that H_2, as LTC suppressor, significantly delays the first-stage ignition in the DF system through reactions $H_2 + OH \rightleftharpoons H + H_2O$, $H + O_2 + (M) \rightleftharpoons HO_2 + (M)$ and $2\,HO_2 \rightleftharpoons H_2O_2 + O_2$. These reactions consume OH radicals, slowing the key H-abstraction reactions of the n-dodecane decomposition. This chemical effect prolongs the first-stage ignition delay time (τ_1^{0D}) and shifts the most reactive first-stage mixture fraction

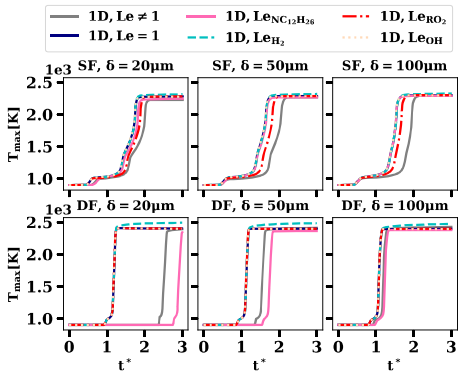

Fig. 8. The temporal evolution of maximum temperature (T_{max}) with different mixing layer thickness (δ).

($\xi^{0D}_{1,mr}$) towards richer mixtures, while the most reactive second-stage mixture fraction (ξ^{0D}_{mr}) remains unchanged.

The two-stage ignition process for the SF and DF cases is examined in 1D simulations. In the SF case, the first-stage ignition initiates at approximately the same mixture fraction and time as in the 0D simulations ($\xi^{0D}_{1,mr}$ and $\tau^{0D}_{1,mr}$). In contrast, for the DF case, first-stage ignition is notably delayed relative to $\tau^{0D}_{1,mr}$. In both cases, diffusion-supported cool flames propagate towards richer mixtures, facilitating the accumulation of key radicals that accelerates the transition to the second-stage ignition. Nevertheless, the onset of second-stage ignition is delayed compared to τ^{0D}_{mr}.

The influence of preferential diffusion varies significantly between SF and DF cases and is strongly affected by the mixing conditions. Under pronounced preferential diffusion, the preferential diffusion of RO_2 slows the onset of second-stage ignition in the SF case but has no discernible impact in the DF case. In both cases, the preferential diffusion of *n*-$C_{12}H_{26}$ delays both the first- and second-stage ignition, while the preferential diffusion of H_2 only increases the maximum flame temperature. In contrast, the preferential diffusion of OH has negligible effects on the ignition process.

From a practical standpoint, the results indicate that hydrogen enrichment can extend ignition delays and improve mixture preparation in dual-fuel engines, potentially supporting more stable and efficient operation. At the same time, the findings highlight the need to carefully control hydrogen blending levels to avoid excessive delays or potential misfire.

Novelty and significance statement

This study provides a comprehensive analysis of the ignition mechanisms in hydrogen/*n*-dodecane dual-fuel mixing layers under engine-relevant conditions, offering novel insights into the combustion dynamics of hydrogen-assisted compression ignition systems. The work highlights the critical influence of hydrogen on delaying the ignition process in dual-fuel configurations compared to single-fuel scenarios due to its consumption of OH radicals during the low-temperature oxidation of *n*-dodecane. Moreover, it identifies the role of diffusion-supported cool flames in accelerating radical accumulation, thus driving the transition to second-stage ignition. A significant contribution is the elucidation of preferential diffusion effects, revealing that *n*-dodecane diffusion dominates the delay in ignition stages, while hydrogen diffusion influences maximum flame temperatures. These findings advance the understanding of the complex interactions governing dual-fuel ignition and provide a robust foundation for optimising hydrogen substitution strategies in heavy-duty engine applications, enhancing both efficiency and sustainability.

CRediT authorship contribution statement

Shibo Gu: Performed research, Analysed data, Drafted the paper. **Armin Wehrfritz:** Supervision, Reviewed the paper. **Evatt R. Hawkes:** Supervision, Provided funding, Reviewed the paper. **Yunchao Wu:** Developed the chemical mechanism, Reviewed the paper. **Tianfeng Lu:** Developed the chemical mechanism, Reviewed the paper. **Haiou Wang:** Supervision, Reviewed the paper.

Declaration of competing interest

The authors declare that they have no known competing financial interests or personal relationships that could have appeared to influence the work reported in this paper.

Acknowledgements

This work was supported by the Australian Renewable Energy Agency (ARENA). Computational resources were provided by the National Computational Infrastructure (NCI Australia) and the Pawsey Supercomputing Centre. These resources were allocated via the National Computational Merit Allocation Scheme and the University of New South Wales. H.W. acknowledges the financial support from National Natural Science Foundation of China (U2441282).

Appendix A. Supplementary data

Supplementary material related to this article can be found online at https://doi.org/10.1016/j.proci.2025.105917.

References

[1] H.L. Yip, A. Srna, A.C.Y. Yuen, S. Kook, R.A. Taylor, G.H. Yeoh, P.R. Medwell, Q.N. Chan, A review of hydrogen direct injection for internal combustion engines: towards carbon-free combustion, Appl. Sci. 9 (22) (2019) 4842.
[2] X. Liu, A. Srna, H.L. Yip, S. Kook, Q.N. Chan, E.R. Hawkes, Performance and emissions of hydrogen-diesel dual direct injection (H2DDI) in a single-cylinder compression-ignition engine, Int. J. Hydrog. Energy 46 (1) (2021) 1302–1314.
[3] Y. Wang, A. Evans, A. Srna, A. Wehrfritz, E. Hawkes, X. Liu, S. Kook, Q.N. Chan, A Numerical Investigation of Mixture Formation and Combustion Characteristics of a Hydrogen-Diesel Dual Direct Injection Engine, Tech. Rep., SAE Technical Paper, 2021.
[4] A. Comandini, N. Chaumeix, J. Maclean, G. Ciccarelli, Combustion properties of n-heptane/hydrogen mixtures, Int. J. Hydrog. Energy 44 (3) (2019) 2039–2052.
[5] H. An, J. Chung, S. Lee, S. Song, The effects of hydrogen addition on the auto-ignition delay of homogeneous primary reference fuel/air mixtures in a rapid compression machine, Int. J. Hydrog. Energy 40 (40) (2015) 13994–14005.
[6] G. Borghesi, E. Mastorakos, R.S. Cant, Complex chemistry DNS of n-heptane spray autoignition at high pressure and intermediate temperature conditions, Combust. Flame 160 (7) (2013) 1254–1275.
[7] S. Sreedhara, K. Lakshmisha, Autoignition in a non-premixed medium: DNS studies on the effects of three-dimensional turbulence, Proc. Combust. Inst. 29 (2) (2002) 2051–2059.
[8] A. Krisman, E.R. Hawkes, M. Talei, A. Bhagatwala, J.H. Chen, A direct numerical simulation of cool-flame affected autoignition in diesel engine-relevant conditions, Proc. Combust. Inst. 36 (3) (2017) 3567–3575.
[9] R.N. Dahms, G.A. Paczko, S.A. Skeen, L.M. Pickett, Understanding the ignition mechanism of high-pressure spray flames, Proc. Combust. Inst. 36 (2) (2017) 2615–2623.
[10] P. Dai, Z. Chen, S. Chen, Ignition of methane with hydrogen and dimethyl ether addition, Fuel 118 (2014) 1–8.
[11] Z. Li, X. Gou, Z. Chen, Effects of hydrogen addition on non-premixed ignition of iso-octane by hot air in a diffusion layer, Combust. Flame 199 (2019) 292–300.
[12] Engine combustion network, 2021, https://www.ca.sandia.gov/ecn/.
[13] G. Borghesi, A. Krisman, T. Lu, J.H. Chen, Direct numerical simulation of a temporally evolving air/n-dodecane jet at low-temperature diesel-relevant conditions, Combust. Flame 195 (2018) 183–202.
[14] C. White, R. Steeper, A. Lutz, The hydrogen-fueled internal combustion engine: a technical review, Int. J. Hydrog. Energy 31 (10) (2006) 1292–1305.
[15] J.H. Chen, A. Choudhary, B. De Supinski, M. DeVries, E.R. Hawkes, S. Klasky, W.-K. Liao, K.-L. Ma, J. Mellor-Crummey, N. Podhorszki, et al., Terascale direct numerical simulations of turbulent combustion using S3D, Comput. Sci. Discov. 2 (1) (2009) 015001.

[16] T. Yao, Y. Pei, B.-J. Zhong, S. Som, T. Lu, K.H. Luo, A compact skeletal mechanism for n-dodecane with optimized semi-global low-temperature chemistry for diesel engine simulations, Fuel 191 (2017) 339–349.
[17] C.-W. Zhou, Y. Li, U. Burke, C. Banyon, K.P. Somers, S. Ding, S. Khan, J.W. Hargis, T. Sikes, O. Mathieu, et al., An experimental and chemical kinetic modeling study of 1, 3-butadiene combustion: Ignition delay time and laminar flame speed measurements, Combust. Flame 197 (2018) 423–438.
[18] D.G. Goodwin, R.L. Speth, H.K. Moffat, B.W. Weber, Cantera: An object-oriented software toolkit for chemical kinetics, thermodynamics, and transport processes, 2018, http://dx.doi.org/10.5281/zenodo.4527812, https://www.cantera.org. Version 2.4.0.
[19] C.K. Law, P. Zhao, NTC-affected ignition in nonpremixed counterflow, Combust. Flame 159 (3) (2012) 1044–1054.
[20] R.J. Kee, M.E. Coltrin, P. Glarborg, Chemically Reacting Flow: Theory and Practice, John Wiley & Sons, 2005.
[21] A. Krisman, E.R. Hawkes, M. Talei, A. Bhagatwala, J.H. Chen, Characterisation of two-stage ignition in diesel engine-relevant thermochemical conditions using direct numerical simulation, Combust. Flame 172 (2016) 326–341.
[22] J.H. Chen, E.R. Hawkes, R. Sankaran, S.D. Mason, H.G. Im, Direct numerical simulation of ignition front propagation in a constant volume with temperature inhomogeneities: I. Fundamental analysis and diagnostics, Combust. Flame 145 (1–2) (2006) 128–144.
[23] H.A. El-Asrag, Y. Ju, Direct numerical simulations of exhaust gas recirculation effect on multistage autoignition in the negative temperature combustion regime for stratified HCCI flow conditions by using H2O2 addition, Combust. Theory Model. 17 (2) (2013) 316–334.